Roll-to-roll nanoimprint lithography of high efficiency Fresnel lenses for micro-concentrator photovoltaics

Alejandra Jacobo-Martín, Norman Jost, Jaime J. Hernández, César Domínguez, Guido Vallerotto, Steve Askins, Ignacio Antón, and Isabel Rodríguez

The article is originally published in Optics Express Vol. 29, Issue 21, pp. 34135-34149 (2021). DOI: https://doi.org/10.1364/OE.437803

Research Article | Vol. 29, No. 21 / 11 Oct 2021 / Optics Express 34135
Optics EXPRESS

Roll-to-roll nanoimprint lithography of high efficiency Fresnel lenses for micro-concentrator photovoltaics

ALEJANDRA JACOBO-MARTÍN,[1] NORMAN JOST,[2] JAIME J. HERNÁNDEZ,[1] CÉSAR DOMÍNGUEZ,[2,3,4] GUIDO VALLEROTTO,[2] STEVE ASKINS,[2] IGNACIO ANTÓN,[2] AND ISABEL RODRÍGUEZ[1,5]

[1]*Madrid Institute for Advanced Studies in Nanoscience (IMDEA Nanoscience), Ciudad Universitaria de Cantoblanco, C/Faraday 9, 28049 Madrid, Spain*
[2]*Instituto de Energía Solar, Universidad Politécnica de Madrid, Av. Complutense 30, 28040 Madrid, Spain*
[3]*ETS Ingeniería y Diseño Industrial, Universidad Politécnica de Madrid, Ronda de Valencia 3, 28012 Madrid, Spain*
[4]*cesar.dominguez@upm.es*
[5]*i.rodriguez@imdea.org*

Abstract: Roll-to-roll nanoimprint lithography (R2R-NIL) is an enabling technology for the low-cost mass production of high-quality micro- and nano-sized optical elements. Particularly, the fabrication of Fresnel lenses using R2R-NIL is a promising approach to produce optical arrays for micro-concentrator photovoltaic modules. This work investigates the application of a continuous R2R imprinting process based on ultraviolet curing of transparent photopolymer resins (UV-NIL) to fabricate high-efficiency and low-cost Fresnel lenses. The morphological attributes and the related optical performance of the lenses fabricated using roll-to-roll UV-NIL on flexible PET sheets yielded optical efficiency values up to ~ 69% at a concentration ratio of 178X, whereas a value of ~ 77% was obtained for the UV-NIL batch processed on a flat rigid substrate. Further improvement of the optical efficiency has been achieved by adding moth-eye inspired antireflective (AR) features on the side opposite to the Fresnel motifs via a double-sided R2R UV-NIL process. The process developed paves the way for cost-effective mass production of high-efficiency Fresnel lenses for micro-concentrator photovoltaics.

1. Introduction

The increasing demand for renewable energy sources has stimulated the continuous development and expansion of photovoltaic (PV) related technologies. Particularly, concentrator photovoltaic (CPV) modules have become a promising solution by concentrating sunlight onto small solar cells using lenses or mirrors, thus reducing semiconductor material consumption and offering the possibility to replace traditional solar cells with more efficient ones like multi-junction (MJ) solar cells [1]. Today, there is a trend for downscaling CPV system dimensions (solar cell and optics) to achieve several gains, such as increasing the optical efficiency of the concentrator optics by reducing the absorption through the optical path and increasing the efficiency of the solar cell by reducing shading caused by the front contacts and temperature losses. The so-called micro-CPV approach consists in CPV systems where the solar cell size is below 1 mm. The reduction in solar cell size implies a proportional reduction in the dimensions of the concentrator optics. On the one hand, the number of (smaller) lenses and cells will be increased quadratically, which introduces the challenge of mass-producing lenses in an inexpensive way. On the other hand, the small lens dimension enables the use of low-cost continuous manufacturing techniques like roll-to-roll (R2R) or roll-to-plate (R2P) nanoimprint lithography (NIL) [2], thus making the whole assembly cost-competitive [3]. Due to their low cost, light weight and short optical

#437803 https://doi.org/10.1364/OE.437803
Journal © 2021 Received 14 Jul 2021; revised 22 Sep 2021; accepted 22 Sep 2021; published 5 Oct 2021

Optics EXPRESS

path, [4] Fresnel lenses are nowadays widely used as light concentration elements in CPV. They are frequently fabricated in polymethylmethacrylate (PMMA) by injection molding [5,6] or by casting optical-grade silicone on a rigid glass substrate [1]. However, either method involves batch processing, which is prohibitively expensive for the sheer number of parts required in micro-CPV [3].

R2R-NIL has been recognized as a promising technology to provide for these benefits in Fresnel lens fabrication [7,8]. It constitutes an advanced technology for continuous manufacturing suitable for mass production of high-quality micro- and nanopatterned flexible substrates, providing for high-throughput and low-cost production. The more traditional injection molding process used for the fabrication of Fresnel lenses consists of several differentiated steps such as filling, molding, cooling, and demolding, which are carried out in batches of small areas. In a R2R-NIL process, all these steps occur sequentially while the polymer film is continuously fed into the imprinting module [9], raising the throughput. There are two main variants of R2R-NIL process [10]. In thermal NIL (R2R T-NIL), the pattern is transferred from a heated mold to a softened thermoplastic polymer [11,12], whereas in the UV-assisted NIL variant (R2R UV-NIL) [13], the patterning material is a low molecular weight photo-resin coated over a web carrier, typically a polyethylene terephthalate (PET) film, imprinted using low pressure, and then cross-linked by UV light. Both approaches have been reported for the fabrication of functional micro- and nanostructures on flexible films [14–18].

Zhang *et al*. [19] and Huang *et al.* [20] reported the fabrication of linear and radial Fresnel lenses respectively on polymer films by R2R UV-NIL using micro-machined roller molds. However, the lenses achieved a light concentration ratio of 16X (*i.e.*, the lens is 16 times larger than the receiver cell) for radial Fresnel lenses, and 4X for linear Fresnel lenses, far below the practical concentration ratios above 100X needed in MJ cell-based CPV modules [1,21]. The optical losses in concentrating optics are related to different factors [22]. On the one hand, there exist defects that produce scattering like surface roughness or waviness and other. On the other hand, shape defects in Fresnel facets like profile errors, tip rounding, or non-right draft angles may modify the light path and defocus the concentrated light spot distribution. In addition, loss mechanisms linked to the optical material like bulk light absorption, surface Fresnel reflections and dispersion are also important [22]. Bulk absorption can be minimized using thin and highly transparent materials. Surface reflectance losses, related to the material refractive index, are often reduced with antireflective (AR) coatings [23].

Although there are several AR solutions, their application to polymeric Fresnel lenses in an effective and low-cost way remains challenging. Zhou *et al.* [24,25] proposed the incorporation of graded refractive index AR coatings based on porous nanomaterials to progressively reduce the refractive index from the lens material to the air. They modified the surface of commercial Fresnel lenses by spin-coating mesoporous silica nanoparticles, improving the lens transmittance and achieving extra functionalities such as antifogging and self-cleaning behavior. Coatings of solid silica nanoparticles were also found to be a low-cost promising approach to improve light transmission for covered Fresnel lenses [26].

Other researchers have centered their studies on surface texturization via subwavelength structures (SWS) inspired by moth eyes. These SWS are typically nano-cone shaped structures that effectively produce a gradual reduction of the refractive index at the surface, being effective for a broad range of wavelengths and incidence angles. C. Steinberg *et al*. [27] and A. Disch *et al.* [28] previously reported some innovative fabrication routes for Fresnel lenses combined with SWS structures by performing firstly a nano-imprinting step of the SWS motifs followed by a UV surface hardening step to finally imprint the Fresnel micro-facets over it. Yanagishita *et al.* [29] fabricated a Fresnel lens including AR nanostructures via NIL using a mold patterned by anodic porous alumina on the dented side of the lens. However, in these works the optical quality of the

Optics EXPRESS

lenses fabricated and the related optical efficiency was not characterized, nor the technology was implemented on a continuous high-throughput process.

In this paper, the fabrication and characterization of highly efficient Fresnel lenses on a highly transparent optical photo-resin by R2R UV-NIL technology is presented. For this, a flexible polymeric working mold was initially prepared in perfluoropolyether (PFPE) [30]. This soft material was found well suited to replicate the original precision machined master mold and at the same time appropriate to imprint the lens with the optical resin with high fidelity. The quality of replication in terms of surface roughness and feature fidelity of the imprinted lenses was characterized by scanning electron microscopy (SEM) and confocal microscopy. The optical performance of the fabricated Fresnel lenses was assessed by measuring their optical efficiency using a solar simulator with a collimated beam to mimic the direct irradiance that would be collected by CPV modules [31] (*i.e.* light coming only from the solar disc) [32]. The reduction of reflectance losses was also explored by incorporating a moth-eye textured AR layer directly on the entrance surface of a lens array without web carrier via a double-sided R2R UV-NIL process.

2. Methods

2.1. Fresnel lens design

The lens design consists in a hexagonal Fresnel lens circumscribing a circle of 16.6 mm in diameter, with a facet height of 50 µm, and a draft angle of 5°. The lenses were designed and optimized to be used with solar cells of 1 mm^2 active area. The area of each single lens is 178 mm^2 resulting in a concentration factor of 178X. The height of 50 µm was defined to guarantee good reproduction during the UV-NIL process. The draft of 5° was selected to facilitate both, the production of the master mold by single-point diamond turning (SPDT) machining as well as the demolding step after the NIL process. The lens profile was obtained by defining a focal distance and a design refractive index. The design refractive index is calculated as the average between the indices for near-UV and near-infrared wavelengths, the edges of the spectral region for which light collection is critical in MJ cells (i.e., top and middle sub-cells, typically limiting the photocurrent of a three-junction MJ cell). This is necessary to minimize losses due to the dispersion of the material used. The process was repeated for several focal distances and all the designed lenses were simulated using Monte Carlo ray-tracing with Synopsis LightTools. The maximum attainable optical efficiency at 178X is 90% according to simulations, including losses due to Fresnel reflections, draft angles, and wavelength-dependent transmittance and refractive indices of the materials involved.

2.2. Preparation of PFPE lens working mold

Soft PFPE based working mold of the Fresnel lens array was replicated from a precision machine brass master (Wielandts UPMT) by soft-lithography followed by UV-NIL process. For this, firstly, polydimethylsiloxane (PDMS) (Sylgard 184, Dow Corning) precursor and initiator degassed mixture (10:1) was cast over the master mold and cured for 24 hours before demolding. Afterwards, a Fluorolink perfluoropolyether MD700 polymer precursor was mixed with 2 wt.% of 2-hydroxy-2-methylpropiophenone (Sigma Aldrich) photoinitiator. The mixture was degassed under vacuum and then was spread over the PDMS replicated structures. The uncured polymer was blanketed with a PET film to avoid polymerization inhibition due to the presence of oxygen. The two layers were then covered with a quartz substrate to homogenize the thickness and exposed to UV light in a chamber (UVASPOT 400/T from Honle) for 5 minutes. Finally, the PFPE working mold was carefully demolded and peeled off from the PDMS and PET film.

Before its use, this PFPE working mold was coated by a silane layer to facilitate the demolding process after imprinting. The silane anti-sticking agent FDTS (perfluorodecyl-trichlorosilane) was applied in gas phase using the procedure reported by Pan *et al.* [33]. For this, 10 µl of 1H,

Optics EXPRESS

1H, 2H, 2H-Perfluorododecyl-trichlorosilane (Alfa Aesar) were poured in an Eppendorf tube and placed close to the PFPE working mold in a closed container. The set was then kept under vacuum at 70 °C overnight to complete the anti-sticking treatment.

2.3. Preparation of moth-eye antireflective working intermediate molds

The working mold to imprint the moth-eye AR topography was prepared by replicating a commercial master nickel mold (HT-AR-02, Temicon) onto a composite PDMS mold. For this, first, a thin layer of hard PDMS (h-PDMS) used to replicate accurately the AR nanocones, was poured onto the nickel mold. The h-PDMS precursor composition was adapted from the work of Schmid *et al.* [34]. This included 6 µl of the catalyst: platinum-divinyltetramethyldisiloxane complex in vinyl terminated poly (dimethylsiloxane) (abcr GmbH) and 100 µl of the modulator: 1,3,5,7-tetravinyl-1,3,5,7-tetramethylcyclotetrasiloxane 97% (abcr GmbH). This mixture was mixed with 3.4 g of a vinyl prepolymer (7-8% Vinylmethylsiloxane - dimethylsiloxane copolymer trimethylsiloxy terminated) (abcr GmbH) and then, 1 g of a hydrosilane prepolymer (Methyl-hydroxisiloxane - dimethylsiloxane copolymer) (abcr GmbH) was added to the mixture and degassed under vacuum before being spread over the master mold. After 15 minutes to allow for the filling of the mold cavities, the remaining polymer was removed by gravity and then, placed in an oven at 80 °C for 20 minutes. After this time, 50 g of s-PDMS (Sylgard 184, Dow Corning) containing a 10:1 ratio precursor-initiator degassed mixture were poured over the partially cured h-PDMS film. The materials were finally cured during 24 hours at 80 °C before demolding the working AR mold of about 3 mm thickness.

This PDMS intermediate mold was replicated by T-NIL on to an intermediate polymer stamp (IPS) film (TIP1, Obducat AB) to produce the final moth-eye AR working mold. The process was performed using an Obducat Eitre 3 NIL tool, applying 45 bars of pressure at 155 °C for 5 minutes. After cooling and demolding, the moth-eye patterned IPS film was ready for the R2R double imprint processes.

2.4. Fresnel lenses fabrication

Fresnel lenses were fabricated on a PET film as support by R2R UV-NIL (samples referred to in this manuscript as FL-PET-R2R) and by traditional plate-based UV-NIL process (FL-PET-REF), the latter to be used as a reference for comparing the impact of the roll-to-roll processing conditions on the concentration efficiency of the lenses. In addition, self-standing (SS) Fresnel lenses were also fabricated with the AR pattern (FL-SS-AR) and without the AR pattern (FL-SS-REF), besides its corresponding reference samples FL-SS-REF and FL-SS-REF-AR prepared by conventional UV-NIL on a plate.

A roll-to-roll equipment (R2R100 Multi, PTMTEC) was used for the fabrication of FL-PET-R2R, FL-SS-R2R and FL-SS-R2R-AR substrates. A highly transparent PET film (Hifi Industrial Film) 10 cm wide and 125 µm thick web was fed into the R2R equipment. For the fabrication of FL-PET-R2R the web was firstly activated by corona discharge (150 W) to improve the adhesion, and subsequently it was coated with an optical photo-resin (FOL 1.2, Film Optics) by blade coating, obtaining a film thickness of about 250 µm, sufficient to fill the facets of the Fresnel lens array of 50 µm in height. Hence, the ratio of lens height to bulk resin support thickness was about 1:7. For the fabrication of FL-SS-R2R and FL-SS-R2R-AR, an IPS flat film or an IPS previously imprinted with the moth-eye AR topography was fixed with a Teflon tape to the PET web carrier (with the motifs facing upwards in the second case) and then, the photo-resin was applied over by blade coating. The R2R UV-NIL process was carried out via horizontal displacement of the web carrier (web tension of 40 N and web speed of 0.05 $m \cdot min^{-1}$), and the PFPE working mold (fixed to the imprinting roller) rolling over the uncured coated photo-resin. The contact area between the mold and the coated surface was exposed to UV-light to cross-link the photo-resin, and the

Optics EXPRESS

web advancing movement facilitated the demolding process. In this case, the ratio of lens height to bulk support thickness was about 1:5.

Reference lenses (FL-PET-REF, FL-SS-REF and FL-SS-REF-AR) were fabricated by low pressure UV-NIL. Firstly, the silanized PFPE working mold placed with the motifs in the upper face was coated with the photo-resin by blade coating. Then, the coated stamp was covered: (i) with a PET film previously activated by oxygen plasma (50W, 1 min, 150 ml·min^{-1} O_2 in a 600 Semi-Auto plasma system, Tepla) for FL-PET-REF, (ii) with a flat IPS film for FL-SS-REF, and (iii) with an IPS moth-eye AR stamp with the motifs in contact to the uncured resin for FL-SS-REF-AR. Following, each set was covered with a quartz piece transparent to UV light, and the whole assembly was exposed to UV-light in a chamber (UVASPOT 400/T from Honle) during 1 min. Finally, the resulting Fresnel lenses were carefully demolded by peeling off the mold.

2.5. Fresnel lenses characterization

Fresnel lenses fabricated were imaged using a scanning electron microscope (SEM) (Auriga FIB-SEM system from Zeiss). Images were taken by a secondary electron detector at low voltage (1 kV).

A dual confocal-interferometry microscope Leica DCM 3D was used to characterize profiles and roughness of Fresnel lenses. A multiple-slit confocal scanning [35] was used to improve signal and accuracy, where the field of view is illuminated with multiple lines rather than a pinhole as in classical confocal microscopy. A high-resolution charge-coupled device (CCD) array is used as metrology sensor, and a high-power white LED as a coaxial light source. The average roughness *R*a at the center of the lens was measured with a resolution better than 2 nm in height and 0,14 µm in the horizontal plane (150X magnification). A length of 60 µm was averaged to display representative values. Profile measurements were evaluated with a vertical resolution better than 3 nm and 0,16 µm in the horizontal plane (50X magnification), measuring the same representative line profile in each lens. Complete lens profiles were obtained using Leica's automatic stitching mode enabled by closed-loop high-precision encoded positioning stages.

Optical efficiency and spot size measurements were carried out using a CPV solar simulator Helios 3198 from Solar Added Value SL [36]. The measurement procedures have been explained visually [37] and described in detail elsewhere [32].

For the optical efficiency measurements, a small 1 mm^2 III-V upright metamorphic triple-junction solar cell was used as a receiver. Its small size requires higher precision alignment than the method presented in the past [38]. To this purpose, linear actuators in all three axes are used to optimize the cell-lens relative position to maximize the short-circuit current (I_{SC}) generated by the device under test (DUT), which is considered a good approximation of the photogenerated current. The DUT is the pair composed of a solar cell and a Fresnel lens and the I_{SC} is defined as the current generated by the solar cell when voltage is equal to 0 V. This procedure is automatized by a MATLAB code. Once the I_{SC} is measured, the resulting efficiency is calculated as shown in Eq. (1). For the spot size measurement, the solar cell is replaced with a Lambertian diffuser, and images of the same are captured by a CCD camera. With image processing the diameter of the spot is calculated by defining the encircled energy value of 95% (this value is chosen to avoid errors caused by noise such as light proceeding from external sources). With the resulting diameter the effective concentration ratio is calculated according to the Eq. (2).

$$\eta_{optical} = \frac{I_{SC,DUT}}{I_{SC,CalibratedAM1.5D} * Geometrical\ concentration} \tag{1}$$

$$Effective\ concentration\ ratio = \frac{Lens\ aperture}{Focal\ spot\ area} = \frac{178mm^2}{\pi * \left(\frac{\emptyset_{spot}}{2}\right)^2} \tag{2}$$

Optics EXPRESS

The reference lens used is from a bulk lens array manufactured by precision glass molding. These lenses are not fresnelized but continuous aspherical due to the molding limitations of glass. Single lenses achieve absolute optical efficiencies of 80% at a concentration of 178X and measured spot sizes of slightly under 1 mm^2 have been reported [39].

3. Results and discussion

3.1. Fresnel lenses fabricated by R2R UV-NIL

3.1.1. Lens array fabrication

The negative-relief Fresnel micro-lens masters were manufactured by SPDT on brass. 24 hexagonal inserts with the same Fresnel lens relief were assembled into a full array of 4×6 rows seen in Fig. 1(a). The profile of the lens design is shown in Fig. 1(b). The fabrication process of SPDT produced an average tip and valley rounding of 3 µm in radius arising from the diamond tool shape.

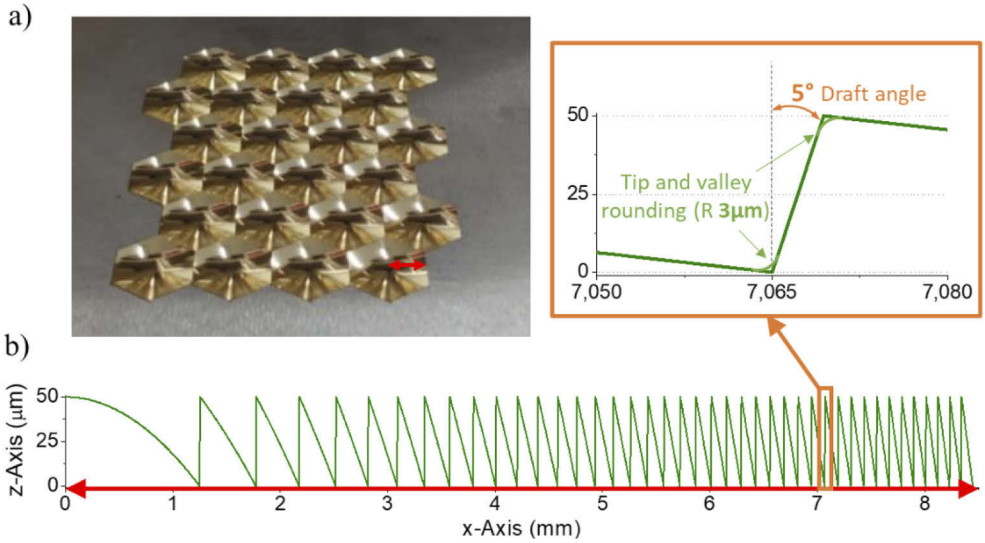

Fig. 1. a) Fresnel lens array master composed of single point diamond turned brass inserts assembled into a full array and b) profile of the Fresnel lens array design.

From this master, soft PFPE working molds were prepared and used for plate and R2R UV-NIL processes. Firstly, the master mold was replicated with polydimethylsiloxane (PDMS) by common soft-lithography [40], and the replica produced was employed to cast a PFPE precursor to fabricate the working mold with the negative Fresnel lens relief via UV photo polymerization For the R2R UV-NIL fabrication of FL-PET-R2R, the mold was fixed to the imprinting roller as shown in Fig. 2(a). Because the photo-resin employed was fast curing, the height of the imprinting roller was configured as close as possible to the UV source and a metal slit was employed to narrow as much as possible the exposed area and limit the cross-linking reactions to the contact line with the imprint mold. In Fig. 2(b) the configuration scheme of the UV-NIL module is presented, where the web and imprinting roller directions are indicated with yellow arrows. The process parameters were adjusted to obtain high fidelity and low defect lens replication. During the R2R process, it was important to optimize the web tension to keep constant and homogeneous the contact area between the coated web and the mold, minimizing the curvature of the PET carrier and avoid causing a longitudinal lens stretching. Also a relative low web speed was selected to

Optics EXPRESS

allow for the elimination of the air within the lens array grooves while the imprinting progressed, hence preventing defects caused by air bubbles trapped within the resin.

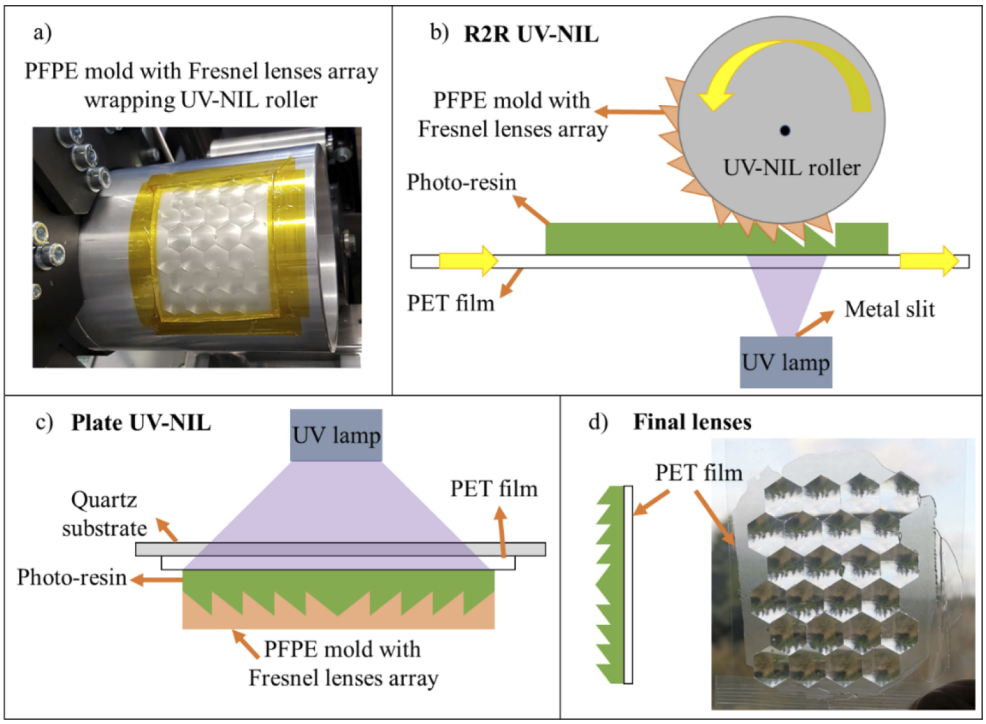

Fig. 2. a) PFPE working mold of the Fresnel lens array fixed on the imprinting roller, b) scheme of R2R UV-NIL process with the web and imprinting roller movement direction marked with yellow arrows, c) scheme of plate UV-NIL, and d) scheme of final lens for both processes with a photograph of a FL-PET-R2R array of lenses.

The reference Fresnel lenses (FL-PET-REF) were fabricated using the traditional plate UV-NIL configuration (see Fig. 2(c)). Figure 2(d) shows schematically the configuration of the final lenses obtained from both plate and R2R UV-NIL processes, where the Fresnel lens fabricated in a photo-resin supported by a PET film. A photograph of the FL-PET-R2R lenses is also displayed. Extended details of the Fresnel lens array fabrication were given in the Methods section.

3.1.2. Lens array characterization

SEM images of the cross-section of both Fresnel lenses fabricated: FL-PET-R2R and FL-PET-REF are shown in Fig. 3(a). It can be appreciated that the lenses present a good surface integrity, a high-fidelity replication of Fresnel lens features, without significant defects derived from the imprint process, such as incomplete filling or deformations associated to demolding forces. To evaluate the replica fidelity and surface finish quality of the imprinted lenses, profile measurements were conducted using noncontact confocal scanning microscopy. Both roughness and geometry of the lens facets were characterized since both parameters have a profound influence on the optical performance [22,41]. The values for the average roughness (*R*a) and tip rounding radius of a sample facet profile are displayed in Table 1. The *R*a value was 5 nm for the master mold according to the manufacturer's metrology, and it was increased up to 8 nm for the reference FL-PET-REF lenses imprinted on a plate, and up to 36 nm in the case of R2R imprinted FL-PET-R2R lenses. The increase in *R*a values on the R2R processed films compared to that of the process on a plate could be associated to the increased imprinting speed. It is possible

Optics EXPRESS

that some portion of the air displaced as the mold cavities were filled remained trapped within the resin, thus increasing surface roughness. The tip rounding radius of the lens facets after the sequential steps of pattern transfer and replication from the original master mold increased from 3 µm in the brass master mold to 7 µm for the final lenses for both the FL-PET-R2R and the reference FL-PET-REF. The fidelity of the imprint process and related lens profile accuracy was characterized by slit confocal scanning microscopy [35] at different areas within the imprinted hexagonal lens array. Figure 3(b) shows a comparison of the first facet profiles obtained for a silicone replica of the original master mold and for the FL-PET-R2R and FL-PET-REF lenses. The profiles match rather well, revealing excellent pattern transfer fidelity during the imprinting process. Mean absolute error (MAE) values compared to the reference mold were estimated to be 0.4 µm and 1.3 µm for the FL-PET-REF and FL-PET-R2R respectively.

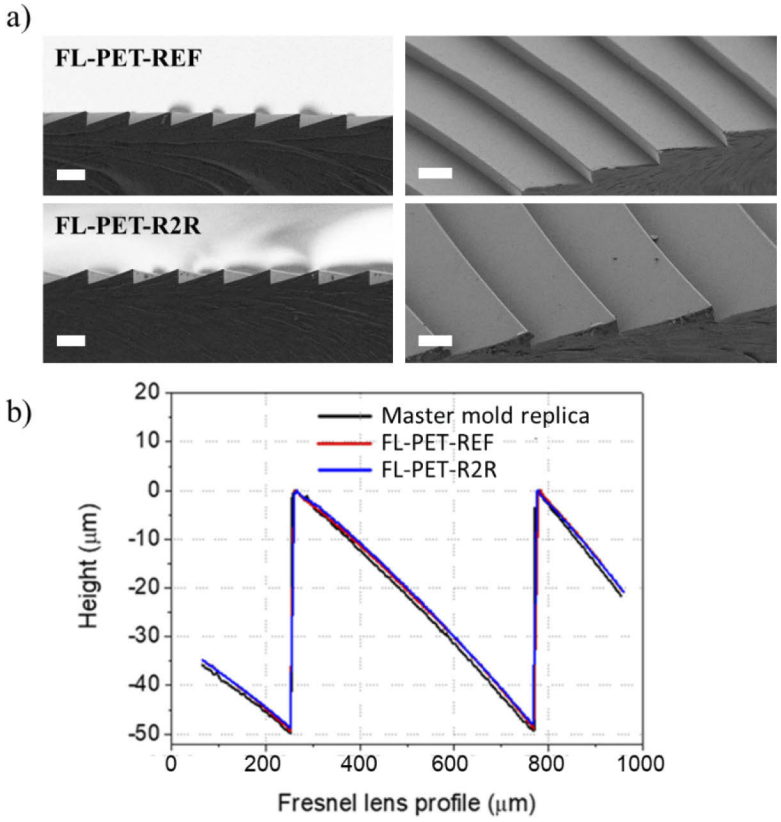

Fig. 3. Geometrical characterization of FL-PET-R2R and FL-PET-REF Fresnel lenses: a) SEM images of the profile (left) and surface (right) (scale bar 100 µm) and b) first facet from center of the Fresnel lens geometrical profile.

The optical performance of the lenses was characterized using a CPV solar simulator. The effective optical efficiency (fraction of incident radiation that is collected by the receiver solar cell, measured through its photocurrent) and the effective concentration ratio (lens area divided by measured spot size) of the lenses were measured using the procedures described in the experimental section and published in detail elsewhere [32,37]. A collimated beam of white light with a spectrum and divergence similar to that of the solar disc is used to illuminate the whole lens array at normal incidence. The effective optical efficiency depends on the area of the receiver used to collect the concentrated light: the larger the receiver, the more light is collected.

Optics EXPRESS

Table 1. Geometrical and optical parameters of the UV-NIL produced lenses[a]

Lens	UV-NIL process	Ra (nm)	Tip Rounding (μm)	Optical efficiency (6X)	Optical efficiency (178X)	Spot size ∅ (mm)	Effective concentration ratio (X)
Holophane	-	-	-	91,1%	80.5%	0.98	236
FL-PET-REF	Plate	8	7	83.3%	76,8%	1.29	135
FL-PET-R2R	R2R	36	7	78.6%	68.7%	1.44	128

[a]The (effective) optical efficiency for two receiver sizes and the effective concentration ratio parameters are compared to a reference aspheric lens (Holophane) [39]. FL-PET-REF: Fresnel lens on PET by UV-NIL on plate used as reference; FL-PET-R2R: Fresnel lens on PET by UV-NIL via R2R

Thus, the geometrical concentration ratio, *i.e.*, the ratio between the area of the lens to that of the receiver, must be specified when measuring the effective optical efficiency (we can simply state 'optical efficiency' for simplicity without ambiguity). Two triple-junction solar cells with different sizes have been used to collect light, which yielded geometrical concentration ratios of 6X and 178X. The size of the concentrated light spot was measured using a Lambertian diffuser and a CCD camera. The values of optical efficiency and effective concentration ratio for the best samples fabricated using plate- or R2R-based UV-NIL are presented in Table 1, compared to those obtained for a commercial non-Fresnel aspheric glass lens with a very high transmittance (Holophane) used as Reference [39].

As shown in Table 1, the optical efficiency of lenses fabricated by R2R UV-NIL (FL-PET-R2R) reached values of 78.62% (at 6X), only ~ 13 percentage points (pp) lower than that of the reference glass lens (91.14%). It is important to note that the non-Fresnel aspheric reference lens has been chosen as the perfect optimum lens, so even if the Fresnel lenses would have been imprinted without any defect, the efficiency would be always lower because of the losses at the interface between facets (*i.e.* tip and valley rounding and draft angle). Comparing to the UV-NIL reference lenses (FL-PET-REF), the optical efficiency obtained at 6X with the R2R imprinted lenses was approx. 5 pp lower (from 83.32% to 78.62%). On the other hand, concerning the optical efficiency values at 178X, a significant decrease was also observed in samples processed with R2R (~ 12 pp compared to ~ 4 pp for the plate-processed lenses). In both cases, the decrease in efficiency can be largely ascribed to the higher roughness of the lenses, which varied from 8 nm in *R*a for the FL-PET-REF lenses to 36 nm for those imprinted by R2R UV-NIL. Nevertheless, Fresnel lenses fabricated by R2R UV-NIL achieved a sunlight concentration ratio of 128X, which is a remarkable increase in optical performance over previous studies: 16X for radial lenses [20].

The results above have been obtained for an optimal focal distance. Figures 4(a) and 4(b) show, respectively the lens optical efficiency and the diameter of the light spot as a function of the cell-lens distance. The results are coherent and show a better performance of the reference UV-NIL lens both in optical efficiency and spot size. Furthermore, despite the measured spot size is slightly bigger than the 1 mm^2 solar cell, most of the energy is concentrated in a reduced area (see meshes in Figs. 4(c) and 4(d)). Therefore, as shown in Fig. 4(a), a negligible efficiency drop is obtained if the cell-lens distance is varied by ±0.8 mm with respect to the optimum position (note the wide plateau of the blue curve – R2R). This increases the tolerance to misalignments in real operation, where the lens temperature changes and so does the material refractive index, which in turn modifies the optimal lens focal distance. This higher tolerance to temperature would increase the energy yield of the CPV module. Finally, in Figs. 4(c) and 4(d) the CCD images of the concentrated spots are plotted as a 3D mesh (left) and 2D projections (right). The 2D projections include the size of the solar cell at 178X and how much the measured spots fill the solar cell area.

Optics EXPRESS

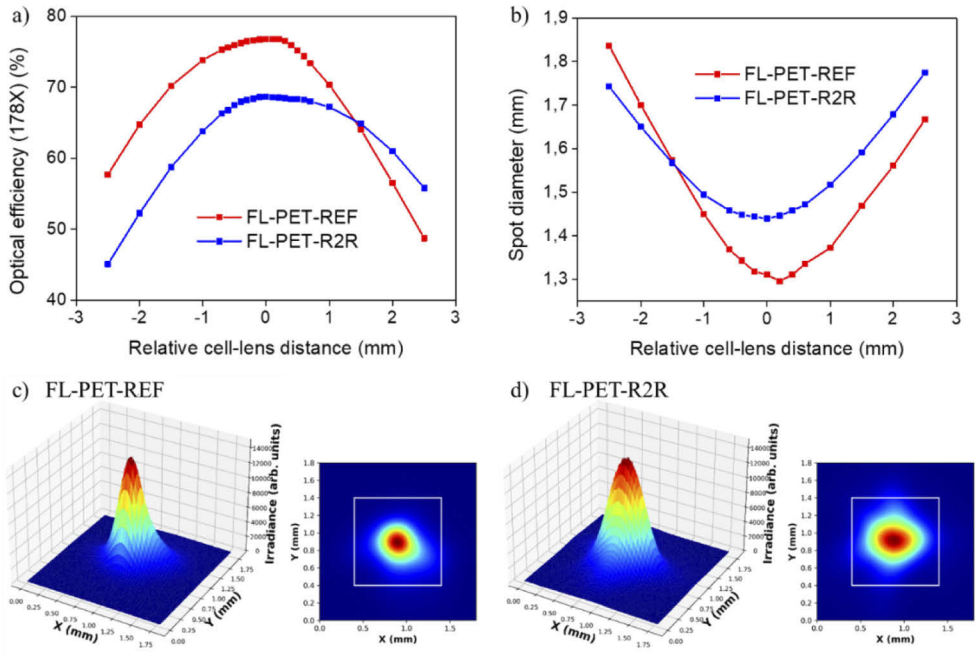

Fig. 4. a) Optical efficiency *vs.* the focal axis at a concentration of 178X for FL-PET-REF and FL-PET-R2R, where an optical efficiency drop of 8 pp is observed for the R2R manufactured lens, b) measured spot size *vs*. the relative cell-lens distance for the same samples, the spot diameter is defined as the circle which contains the 95% of the energy collected by the receiver. In both figures a) and b), the x-axis represents the relative cell-lens distance, where zero is the optimal position, which is defined as the cell-lens distance that maximizes the efficiency (and minimizes the spot diameter). c) and d) 3D mesh plots (left) and 2D projections (right) of the captured spot for FL-PET-REF and FL-PET-R2R, respectively. The increase of spot size diameter is of 0.15 mm, which decreases the concentration ratio by 25X, the square seen in the 2D projection represents the size of the 1 mm^2 solar cell.

3.2. Fresnel lens with AR topography fabricated by double-sided R2R-NIL

3.2.1. Fabrication process

Further improvement of the optical efficiency was attempted by the incorporation of a moth-eye AR texture on the entrance surface of a self-standing lens array to obtain a reduction of reflectance loss at this interface. In this case, the lenses were fabricated as self-standing (SS) arrays, that is, without the PET substrate to avoid an extra interface and the associated light loss (FL-SS-R2R-AR). A double-sided R2R UV-NIL process was developed for this purpose. Initially, a working mold containing the AR nano-features was fabricated by thermal NIL on a UV transparent, low surface-energy intermediate polymer stamp (IPS) thermoplastic film. This working mold was fixed on the R2R PET carrier web and then coated with the photo-resin by blade coating. Subsequently, the resin was roll-imprinted with the PFPE mold having the Fresnel lens negative array wrapped around the roller as shown in Fig. 5(a). As the web advanced, the resin was cured by the UV-light coming from below. At the end of the imprinting process, a self-standing film with the Fresnel lens array on one side and the AR topography on the opposite side, was easily demolded and released from the IPS substrate. Self-standing Fresnel lenses without the AR pattern (FL-SS-R2R) were also fabricated as reference using the same procedure but, in this case, using a flat IPS film. Reference samples FL-SS-REF and FL-SS-REF-AR were prepared by conventional UV-NIL on a plate, with the setup shown in Fig. 5(b). In Fig. 5(c) it

Optics EXPRESS

is shown a schematic of the resulting Fresnel lens and a photograph of FL-SS-R2R-AR film obtained.

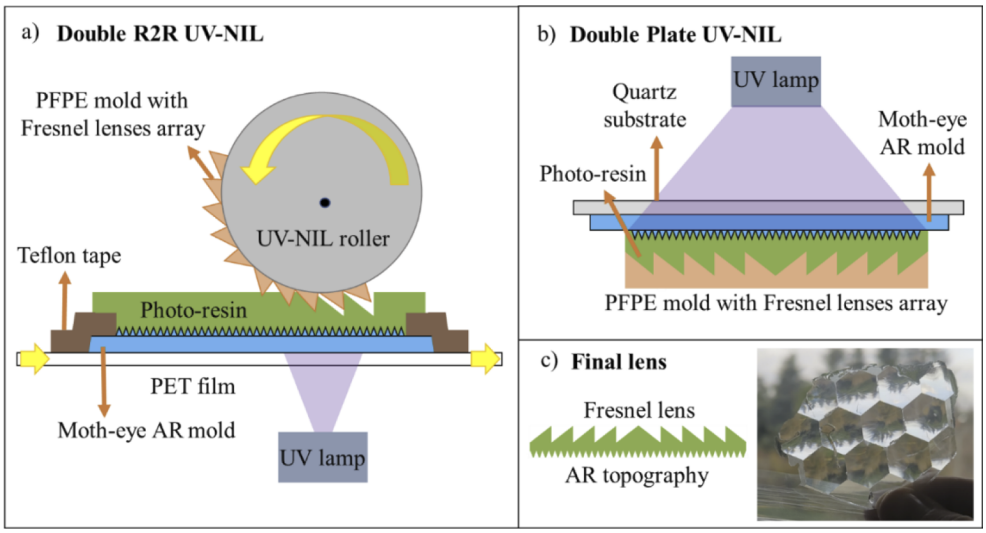

Fig. 5. a) Scheme of double-sided R2R UV-NIL process, b) scheme of the double-sided plate UV-NIL, and c) scheme of final lens for both processes and a photograph of FL-SS-R2R-AR.

3.2.2. Lens array characterization

Figure 6(a) shows a SEM image of a lens FL-SS-R2R-AR, where it can be appreciated that both the micro- and AR nano-topography were imprinted with high fidelity. (A detailed description of the imprinted moth-eye nano-features is provided in Supplement 1 Figure S1). Figure 6(b) shows the first facet of the Fresnel lens profile comparing FL-PET-R2R, FL-SS-R2R-AR and the silicone copy of the master mold. These three profiles show a high-fidelity match (MAE = 0.6 μm for the FL-SS-R2R-AR lenses), indicating that the double imprinting process does not reduce the pattern transfer accuracy. Figure 6(c) shows the self-standing lens optical efficiency at 178X as a function of the cell-lens distance. A similar trend to that observed in the PET supported membranes, with a limited efficiency drop for ±0.8 mm cell-lens distance variation, is confirmed.

*R*a values are presented in Table 2, where it can be appreciated the same tendency described before; the lenses prepared via plate-based UV-NIL presented lower *R*a values, while the R2R processing produced higher *R*a results. This higher roughness can be assumed to be intrinsically related to the R2R process, with no significant differences between the single- and double-sided imprinting processes.

The transmittance values of a self-standing ~ 200 μm thickness photo-resin film improved from ~ 90% to ~ 93% (~ 3% within the range 400 to 700 nm) by imprinting the AR topography on its surface (see Supplement 1 Figure S2a). As such, the AR topography improves the effective optical efficiency of the self-standing lenses by reducing by a similar amount the losses due to light reflection. Nonetheless, due to diffraction by the moth-eye hexagonal lattice and the subsequent coupling of light into the higher-order propagating modes of the substrate, we observe a transmittance dip below 400 nm (see Supplement 1 Figure S2b). This will introduce a loss in the optical efficiency of the lens for near-ultraviolet light, however, the fraction of solar power in this spectral region is small (3%) and very often real-world CPV module designs use encapsulation materials that filter UV to reduce weathering. All in all, the expected losses due to diffractive coupling by the AR layer at near-UV should be well below 1%.

Optics EXPRESS

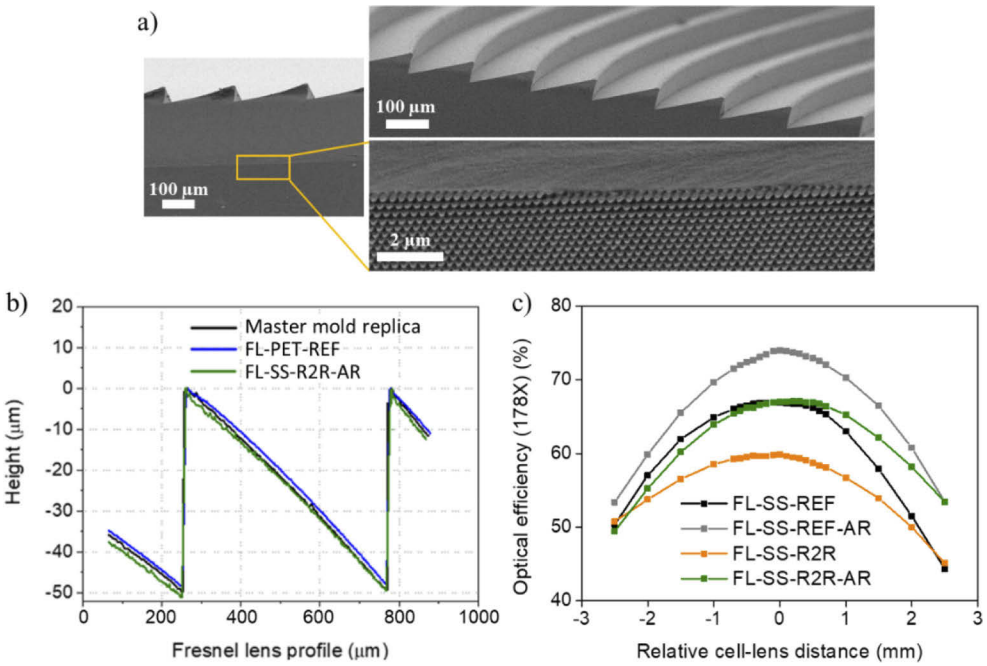

Fig. 6. Geometrical characterization of FL-SS-R2R-AR Fresnel lenses: a) SEM images of the profile (left) and surface (right: top for Fresnel facets and bottom for moth-eye AR nanostructure); b) a sample profile of the first facet from the center of the Fresnel lens; c) Optical efficiency *vs.* the focal axis at a concentration of 178X for FL-SS-REF, FL-SS-REF-AR, FL-SS-R2R and FL-SS-R2R-AR.

The equivalent profiles measured in plate and R2R UV-NIL fabricated lenses (cf. Figure 6(b)) make it reasonable to assume that the double-sided imprinted lenses should achieve a similar concentration ratio. The effective optical efficiency was measured by following the procedure explained before, and the corresponding results are displayed in Table 2.

The effective optical efficiency at 6X obtained for the FL-SS-R2R-AR lenses reached values up to ~ 86%. An improvement of ~ 5 pp efficiency was presumed to be related to the reduction of reflectance loss by the AR topography, and it was observed in both sets of lenses, FL-SS-REF-AR and FL-SS-R2R-AR, relative to the equivalent lenses without the AR topography.

Table 2. Geometrical and optical characterization parameters of the double-sided UV-NIL produced lenses.[a]

Lens	UV-NIL process	*R*a (nm)	Optical efficiency (6X)	Optical efficiency (178X)
Holophane	N/A	-	91.1%	80.5%
FL-SS-REF	Plate	9 nm	79.5%	66,9%
FL-SS-REF-AR	Plate	6 nm	84.6%	73.9%
FL-SS-R2R	R2R	23 nm	81.2%	59.9%
FL-SS-R2R-AR	R2R	34 nm	86.0%	67.1%

[a]Effective optical efficiency values are compared to a reference aspheric glass lens (Holophane) [39]. FL-SS-REF: Fresnel lens self-standing by UV-NIL on plate used as reference; FL-SS-REF-AR: Fresnel lens self-standing by UV-NIL on plate with antireflective texture; FL-SS-R2R: Fresnel lens self-standing by UV-NIL via R2R; FL-SS-R2R-AR : Fresnel lens self-standing by UV-NIL via R2R with antireflective texture

Optics EXPRESS

Unlike in results presented in Table 1, in this case upscaling the imprint process via R2R did not affect substantially the optical efficiency (79.48% for FL-SS-REF and 81.20% for FL-SS-R2R at 6X). However, both FL-SS-REF and FL-SS-R2R were somewhat less efficient than the lenses standing on the PET film (FL-PET-REF). Having an additional layer of PET in this case would theoretically lead to a decrease in efficiency due to an increased bulk absorption and the reflectance loss at the extra interface. However, it is possible that the additional PET film helps to increase flatness on the self-standing lenses patterned on the thin flexible films. Thus, considering the different factors, it is reasonable to obtain for both lenses an optical efficiency value intermediate between FL-PET-REF and FL-PET-R2R.

Comparing the optical efficiency of the lenses on a PET film to that of the self-standing ones, a larger variability is seen at 178X than at 6X. This can imply that the film substrate improves process repeatability and prevents lens warping after curing.

To incorporate self-standing or PET film-supported Fresnel lenses in practical micro-CPV modules, a subsequent lamination step on a glass or PMMA substrate would be required.

4. Conclusions

Polymer Fresnel lenses were successfully fabricated by R2R UV-NIL technology. The process allowed for high fidelity replication, low surface roughness (Ra ~ 35 nm), and low tip rounding (~7 μm radius). The optical performance of the lenses was characterized using a CPV solar simulator. High optical efficiency values were achieved for the R2R produced lenses at low concentration (6X), being just ~ 13 pp lower than that of a reference non-Fresnel aspheric lens (91.14% *vs.* 78.53%). Values at 178X varied from 80.56% to 64.88% (~ 16 pp). A maximum concentration of 128X was achieved, improving remarkably from 16X as the best result reported. In addition, polymer Fresnel lenses with moth-eye AR topography on its reverse side were successfully fabricated by R2R double-sided imprinting. High quality pattern transfer was achieved, and an improvement of ~ 5 pp efficiency with respect to the lenses without AR topography was attained. An optical efficiency of ~ 86% was accomplished, just ~ 5 pp less than that of the reference glass aspheric lens. The warping effect found in self-standing lenses would be removed upon lamination on glass or PMMA substrates for a realistic integration in micro-CPV systems.

In summary, this study proposes a low-cost, high-throughput fabrication route for the manufacturing of high-efficiency Fresnel lenses on flexible substrates with reduced reflectance losses via the incorporation of an antireflective layer using a double-sided R2R UV-NIL process that is fast and suitable for mass production.

Funding. Comunidad de Madridunder the project MADRID-PV2 (P2018/EMT-4308, PEJD-2017-PRE/IND-3788); Ministerio de Economía y Competitividad 'Severo Ochoa' Programme for Centres of Excellence in R&D (SEV-2016-0686); Ministerio de Ciencia, Innovación y Universidades under the project Micro-PV (ENE2017-87825-C2-1-R).

Disclosures. The authors declare no conflicts of interest.

Data availability. Data underlying the results presented in this paper are not publicly available at this time but may be obtained from the authors upon reasonable request.

Supplemental document. See Supplement 1 for supporting content.

References

1. M. Wiesenfarth, I. Anton, and A. W. Bett, "Challenges in the design of concentrator photovoltaic (CPV) modules to achieve highest efficiencies," Appl. Phys. Rev. **5**(4), 041601 (2018).
2. H. Tan, A. Gilbertson, and S. Y. Chou, "Roller nanoimprint lithography," J. Vac. Sci. Technol. B **16**(6), 3926–3928 (1998).
3. C. Domínguez, N. Jost, S. Askins, M. Victoria, and I. Antón, "A review of the promises and challenges of micro-concentrator photovoltaics," AIP Conf. Proc. **1881**, 080003 (2017).
4. R. Leutz and A. Suzuki, "Nonimaging Fresnel Lenses: Design and Performance of Solar Concentrators," in *Nonimaging Fresnel Lenses: Design and Performance of Solar Concentrators*, R. Leutz and A. Suzuki, eds. (Springer Berlin Heidelberg, Berlin, Heidelberg, 2001).

Optics EXPRESS

5. T. Luce and J. Cohen, "The path to volume production for CPV optics," *2010 35th IEEE Photovoltaic Specialists Conference*, 000487–000492 (2010).
6. R. Mohedano and R. Leutz, "CPV Optics," in *Handbook of Concentrator Photovoltaic Technology*John Wiley and Sons, Ltd. (2016), pp. 187–238.
7. L. Peng, Y. Deng, P. Yi, and X. Lai, "Micro hot embossing of thermoplastic polymers: a review," J. Micromech. Microeng. **24**(1), 013001 (2014).
8. S. Meng, Z. Yin, Y. Guo, J. Yao, and N. Chai, "Ultra-precision machining of polygonal Fresnel lens on roller mold," Int J Adv Manuf Technol **108**(7-8), 2445–2452 (2020).
9. N. Kooy, K. Mohamed, L. T. Pin, and O. S. Guan, "A review of roll-to-roll nanoimprint lithography," Nanoscale Res Lett **9**(1), 320 (2014).
10. A. Schleunitz, C. Spreu, T. Mäkelä, T. Haatainen, A. Klukowska, and H. Schift, "Hybrid working stamps for high speed roll-to-roll nanoreplication with molded sol–gel relief on a metal backbone," Microelectron. Eng. **88**(8), 2113–2116 (2011).
11. T. Mäkelä, T. Haatainen, P. Majander, J. Ahopelto, and V. Lambertini, "Continuous Double-Sided Roll-to-Roll Imprinting of Polymer Film," Jpn. J. Appl. Phys. **47**(6), 5142–5144 (2008).
12. T. Makela, V. Lambertini, T. Haatainen, P. Majander, and J. Ahopelto, "Continuous 2-Sided Roll to Roll Nanopatterning of a Polymer Film," in *2007 Digest of papers Microprocesses and Nanotechnology*, 426–427, IEEE (2007).
13. S. H. Ahn and L. J. Guo, "Large-Area Roll-to-Roll and Roll-to-Plate Nanoimprint Lithography: A Step toward High-Throughput Application of Continuous Nanoimprinting," ACS Nano **3**(8), 2304–2310 (2009).
14. A. Jacobo-Martín, M. Rueda, J. J. Hernández, I. Navarro-Baena, M. A. Monclús, J. M. Molina-Aldareguia, and I. Rodríguez, "Bioinspired antireflective flexible films with optimized mechanical resistance fabricated by roll to roll thermal nanoimprint," Sci. Rep. **11**(1), 2419 (2021).
15. A. Retolaza, A. Juarros, J. Ramiro, and S. Merino, "Thermal roll to roll nanoimprint lithography for micropillars fabrication on thermoplastics," Microelectron. Eng. **193**, 54–61 (2018).
16. N. Unno, T. Mäkelä, and J. Taniguchi, "Thermal roll-to-roll imprinted nanogratings on plastic film," Journal of Vacuum Science & Technology B **32**(6), 06FG03 (2014).
17. C.-J. Ting, F.-Y. Chang, C.-F. Chen, and C. P. Chou, "Fabrication of an antireflective polymer optical film with subwavelength structures using a roll-to-roll micro-replication process," J. Micromech. Microeng. **18**(7), 075001 (2008).
18. S. Khandavalli, P. Rogers, and J. P. Rothstein, "Roll-to-roll fabrication of hierarchical superhydrophobic surfaces," Appl. Phys. Lett. **113**(4), 041601 (2018).
19. X. Zhang, K. Liu, X. Shan, and Y. Liu, "Roll-to-roll embossing of optical linear Fresnel lens polymer film for solar concentration," Opt. Express **22**(S7), A1835–A1842 (2014).
20. R. Huang, X. Zhang, B. P. Ng, A. S. Kumar, and K. Liu, "Roll-to-Roll Embossing of Optical Radial Fresnel Lenses on Polymer Film for Concentrator Photovoltaics: A Feasibility Study," Int. J. of Precis. Eng. and Manuf.-Green Tech. **8**(1), 77–88 (2021).
21. E. Menard, M. Sullivan, J. Wilson, B. Fisher, S. Seel, M. Meitl, K. Ghosal, and S. Burroughs, *Optics development for micro-cell based CPV modules, SPIE Solar Energy + Technology* (SPIE, 2011), Vol. 8108.
22. A. Ritou, P. Voarino, and O. Raccurt, "Does micro-scaling of CPV modules improve efficiency? A cell-to-module performance analysis," Sol. Energy **173**, 789–803 (2018).
23. N. Shanmugam, R. Pugazhendhi, R. Madurai Elavarasan, P. Kasiviswanathan, and N. Das, "Anti-Reflective Coating Materials: A Holistic Review from PV Perspective," Energies **13**(10), 2631 (2020).
24. G. Zhou, J. He, and L. Xu, "Antifogging antireflective coatings on Fresnel lenses by integrating solid and mesoporous silica nanoparticles," Microporous Mesoporous Mater. **176**, 41–47 (2013).
25. G. Zhou, J. He, L. Gao, T. Ren, and T. Li, "Superhydrophobic self-cleaning antireflective coatings on Fresnel lenses by integrating hydrophilic solid and hydrophobic hollow silica nanoparticles," RSC Adv. **3**(44), 21789–21796 (2013).
26. G. Zhou and J. He, "Antireflective coatings on Fresnel lenses by spin-coating of solid silica nanoparticles," J. Nanosci. Nanotechnol. **13**(8), 5534–5541 (2013).
27. C. Steinberg, N. Al-Hussainawi, M. Papenheim, A. Mayer, H.-C. Scheer, M. Matschuk, and H. Pranov, "Low reflection Fresnel lenses via double imprint combined with vacuum-UV surface hardening," Journal of Vacuum Science & Technology B **35**(6), 06G306 (2017).
28. A. Disch, J. Mick, B. Bläsi, and C. Müller, "Nanostructures on microstructured surfaces," Microsyst. Technol. **13**(5-6), 483–486 (2007).
29. T. Yanagishita, K. Nishio, and H. Masuda, "Anti-Reflection Structures on Lenses by Nanoimprinting Using Ordered Anodic Porous Alumina," Appl. Phys. Express **2**, 022001 (2009).
30. J. John, Y. Tang, J. P. Rothstein, J. J. Watkins, and K. R. Carter, "Large-area, continuous roll-to-roll nanoimprinting with PFPE composite molds," Nanotechnology **24**(50), 505307 (2013).
31. C. Domínguez, I. Antón, and G. Sala, "Solar simulator for concentrator photovoltaic systems," Opt. Express **16**(19), 14894–14901 (2008).
32. M. Victoria, S. Askins, R. Herrero, I. Antón, and G. Sala, "Assessment of the optical efficiency of a primary lens to be used in a CPV system," Sol. Energy **134**, 406–415 (2016).
33. Z. Pan, H. Shahsavan, W. Zhang, F. K. Yang, and B. Zhao, "Superhydro-oleophobic bio-inspired polydimethylsiloxane micropillared surface via FDTS coating/blending approaches," Appl. Surf. Sci. **324**, 612–620 (2015).

Optics EXPRESS

34. H. Schmid and B. Michel, "Siloxane Polymers for High-Resolution, High-Accuracy Soft Lithography," Macromolecules **33**(8), 3042–3049 (2000).
35. C. J. Koester, "Comparison of Various Optical Sectioning Methods," in *Handbook of Biological Confocal Microscopy*, J. B. Pawley, ed. (Springer US, Boston, MA, 1995), pp. 525–534.
36. K. Larsson, "Cubic Llpid-Water Phases: Structures and Biomembrane Aspects," J. Phys. Chem. **93**(1), 10–12 (1989).
37. G. Vallerotto, M. Victoria, S. Askins, R. Herrero, C. Domínguez, I. Antón, and G. Sala, "Design and modeling of a cost-effective achromatic Fresnel lens for concentrating photovoltaics," Opt. Express **24**(18), A1245–A1256 (2016).
38. G. Vallerotto, M. Victoria, S. Askins, I. Antón, G. Sala, R. Herrero, and C. Domínguez, "Indoor Experimental Assessment of the Efficiency and Irradiance Spot of the Achromatic Doublet on Glass (ADG) Fresnel Lens for Concentrating Photovoltaics," JoVE, e56269 (2017).
39. N. Jost, G. Vallerotto, A. Tripoli, B. D. L'Eprevier, C. Domínguez, S. Askins, and I. Antón, "Molded glass arrays for micro-CPV applications with very good performance," AIP Conf. Proc. **2298**, 050003 (2020).
40. I. Rodríguez and J. Hernández, "Soft thermal nanoimprint and hybrid processes to produce complex structures," in *Nanofabrication* (IOP Publishing, 2020), Chap. 7-1, pp. 7–33.
41. X. Zhang, R. Huang, K. Liu, A. S. Kumar, and X. Shan, "Rotating-tool diamond turning of Fresnel lenses on a roller mold for manufacturing of functional optical film," Precision Engineering **51**, 445–457 (2018).